Understanding Cage Effects in Imidazolium Ionic Liquids by ^{129}Xe NMR: MD Simulations and Relativistic DFT Calculations

Giacomo Saielli,*[,†] Alessandro Bagno,[‡] Franca Castiglione,[§] Roberto Simonutti,[∥] Michele Mauri,[∥] and Andrea Mele*[,§,⊥]

[†]CNR − Istituto per la Tecnologia delle Membrane, Unità di Padova, Via Marzolo, 1, 35131 Padova, Italy

[‡]Dipartimento di Scienze Chimiche, Università di Padova, Via Marzolo 1, 35131 Padova, Italy

[§]Department of Chemistry, Materials and Chemical Engineering "G. Natta", Politecnico di Milano, Piazza L. Da Vinci, 32, 20133 Milano, Italy

[∥]Dipartimento di Scienza dei Materiali, Università degli Studi di Milano Bicocca, Via Roberto Cozzi, 55, 20125 Milano, Italy

[⊥]CNR − Istituto di Chimica del Riconoscimento Molecolare, Via L. Mancinelli, 7, 20131 Milano, Italy

1. INTRODUCTION

Room-temperature ionic liquids (RTILs or simply ILs) continue to raise an impressive interest in the scientific community owing to their growing fields of technological applications (biomass processing,[1] gas separations,[2] nanomaterial synthesis,[3] electrochemistry,[4] and energy storage[5]), which prompts for thorough experimental and theoretical studies of their structural properties at the molecular level. ^{129}Xe NMR spectroscopy[6] of Xe dissolved in ILs was recently applied to a collection of model alkylimidazolium-based ILs,[7,8] and it was demonstrated that it could provide direct and unique information on some aspects of the local structure of ILs. On the one hand, it was pointed out that ^{129}Xe chemical shift is influenced by the size and structure of the apolar domains[9] within the liquid; it is, therefore, a useful probe to monitor the morphology changes that the apolar domains undergo by varying of the alkyl chain length on the imidazolium ring.[7] On the other hand, it was shown that the ^{129}Xe chemical shift of Xe dissolved in imidazolium ILs with different anions [I, Br, Cl, AcO, NO_3, BF_4, PF_6, Tf_2N] exhibits a strong anion dependence, with higher δ values upon going from Tf_2N to the halides and a 100 ppm dispersion.[8] A possible rationale for this trend relies upon the well-recognized sensitivity of the ^{129}Xe chemical shift on the free volume available for its confinement;[10] the smaller the available free volume, the higher the chemical shift value (i.e., deshielding) with respect to gas-phase Xe taken as reference. This fact implies that ^{129}Xe NMR spectroscopy may be used, in principle, as a probe of the available free volume in ILs. The notion of free volume is well established in polymer science, where it is regarded as "a real physical object characterized by an average size and shape of the "hole" (a free-volume element, FVE), FVE size distribution, topology, and connectivity (closed or open internal porosity)";[11] in contrast, the key role played by the empty voids within ILs has been stressed to account for unique properties of ILs only recently. Two paradigmatic examples may be reported here, (i) the ability of imidazolium-based ILs to absorb large quantities of CO_2 without appreciable volume expansion of the liquid phase[12,13] and (ii) the non-Stokesian behavior observed in the transport properties of many ILs.[14] The free volume arguments invoked by some of us[8] to rationalize the observed trend of the ^{129}Xe chemical shift of imidazolium ILs mentioned above find an interesting correspondence with the experimental average local free volume ("hole" volumes, referred to as $\langle v_h \rangle$) obtained by the measurement of the positron decay spectra (positron annihilation lifetime spectroscopy, PALS) in a similar collection

Received: November 9, 2014
Revised: November 13, 2014
Published: November 13, 2014

of imidazolium-based ILs.[15−17] Indeed, the hole volumes $\langle v_h \rangle$ reported by Yu et al.[16] for bmim ILs show the order [Cl] < [BF_4] < [PF_6] < [Tf_2N], thus perfectly matching with the decreasing ^{129}Xe chemical shift of the same set of ILs at the same temperature, δ[Cl] > δ[BF_4] > δ[PF_6] > δ[Tf_2N].

In order to shed more light on the role of voids and cage effects on the ^{129}Xe chemical shift in ILs, we report on a computational study, based on molecular dynamics simulation and relativistic DFT chemical shift calculations, of two ILs, Xe@[bmim][Cl] and Xe@[bmim][PF_6]. These two systems have been selected from the experimental work of Castiglione et al.[8] because they show a relatively large difference in ^{129}Xe chemical shift of about 40 ppm, with Xe@[bmim][PF_6] being more shielded. On the other hand, we have excluded the more deshielding but polarizable bromide and iodide imidazolium salts to avoid possible effects due to the anion polarizability and the more shielding bistriflimide salt to avoid possible complications due to the anion flexibility.[18] The purpose of the investigation is two-fold, (i) characterizing the xenon cage in the two ILs and the cage volumes distribution by MD simulation and (ii) using DFT calculation of the ^{129}Xe chemical shift on clusters extracted from the MD trajectories for comparison with experimental data.

2. THEORETICAL METHODS

MD simulations were run with the software DLPOLY Classic[19] using the fully atomistic force field of Canongia Lopes et al.[20,21] for [bmim][Cl] and [bmim][PF_6], while Xe parameters were taken from ref 22. The same parametrization has been used by Morgado et al. in ref 7, where some imidazolium ILs were investigated by MD but not the [bmim] systems studied here; see Figure 1 for labeling.

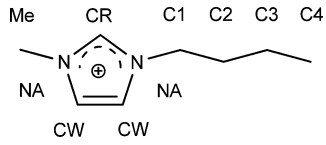

Figure 1. Structure and atom labels of the [bmim] cation.

For both systems, the initial box was prepared from scratch by placing 165 ion pairs and a Xe atom in a rectangular box with a large volume to avoid overlap and equilibrating at high temperature for 10000 time steps with an integration step of 0.5 fs. Then, the system was equilibrated at 800 K and 1 atm in the *NPT* ensemble for 1000000 time steps (500 ps). From this trajectory, two initial configurations were taken, at 250 ps and at the end, and used as starting configurations for two independent *NPT* runs at 500 K and 1 atm, following the protocol used by Morgado et al.[7] The two simulations, for each ionic liquid, lasted for 6 ns, and the analysis was performed on the last 5 ns for a total of 10 ns of trajectory for each ionic liquid. Leapfrog integrator and the Hoover thermostat and barostat were used, with a cutoff radius for the van der Waals interactions of 16 Å. Ewald summation with a precision of 10^{-6} was used for the electrostatic interactions. The relatively high temperature, which is the same as that used in ref 7, is necessary to speed up the dynamics, which is known to be slowed down significantly by electrostatic interactions in nonpolarizable force fields compared to real systems.[23,24] Configurations were saved in the trajectory files every 0.5 ps, for a total of 10000 configurations for each trajectory (20000 for each ionic liquid from the two independent runs). These configurations were used for subsequent analysis and to select clusters for DFT calculations. Unless otherwise stated, average properties were calculated over the two independent runs.

Relativistic DFT calculations were run with the software ADF 2013.[25] These protocols have demonstrated a high level of accuracy in predicting NMR properties of xenon in several environments.[26,27] Clusters were obtained by selecting all molecules for which at least one atom was inside of a radius R from the Xe atom. In a few cases, we tested the effect of the cluster size by comparing the results of R = 6.0 and 7.37 Å (corresponding to the first minimum of the radial distribution function). These tests were run with the TZ2P basis set for Xe and DZP basis set for the surrounding ions. The results were within a few ppm, which was expected to be much below the final accuracy of the results. Therefore, we considered the radius of 7.37 Å to represent a sufficient size to obtain reliable results. Then, we verified that reducing the basis set to the smaller TZP for Xe and DZ for the surrounding ions only amounted to a systematic effect of about 10 ppm, which is expected to cancel out in the calculation of the relative shielding of Xe in [bmim][Cl] and [bmim][PF_6]. Therefore, we used clusters corresponding to a radius of 7.37 Å and the small basis set TZP for Xe and DZ for [bmim][X] for the rest of the calculations, together with the BLYP functional at the scalar relativistic level. Although spin−orbit coupling is known to be important in the calculation of NMR properties of heavy atoms, the relative shift for analogous systems is expected to be very similar; thus, it will not contribute to the relative chemical shift of xenon in [bmim][X].[27]

For Xe@[bmim][PF_6], the clusters were taken at regular intervals every 500 ps. For all of them, the SCF procedure converged smoothly. In contrast, for Xe@[bmim][Cl], we sometimes encountered problems in the SCF convergence, which could not be remedied even employing the usual strategies recommended in such cases. This problem is probably related to the occurrence of near-degenerate molecular orbitals located on very different regions of this complex system, mediated by the polarizable chloride. In such cases, clusters at different time steps had to be selected; however, the clusters for which the SCF procedure converged represent an unbiased average distribution of volumes and charges, as will be shown in the Results and Discussion section.

3. RESULTS AND DISCUSSION

3.1. MD Simulations and Cage Calculations. In Figures 2 and 3, we show the radial distribution functions of Xe with some of the atoms of [bmim][X].

We note that in both ionic liquids, Xe has a weak interaction with the imidazolium ring, as judged by the absence of a strong peak in the $g(r)$ Xe−CR, where CR is the carbon atom in position 2 of the imidazolium ring. In contrast, there is a clear interaction with the butyl chains, as we can see from the increasing height of the peak at around 4 Å as we move toward the methyl group of the chain. The interaction with the butyl chains is more evident for the chloride system, for which, on the other hand, we also observe a rather weak interaction of Xe with the chloride anion. In contrast, a relatively sharp peak is observed in the $g(r)$ between Xe and P in [bmim][PF_6]. Due to the sensitivity of the chemical shift on charge distribution, it is of interest to introduce a radial charge distribution function, $\rho(r)$, around the xenon atom. This can be interpreted as the analogue of the total radial distribution function $g(r)$ but now

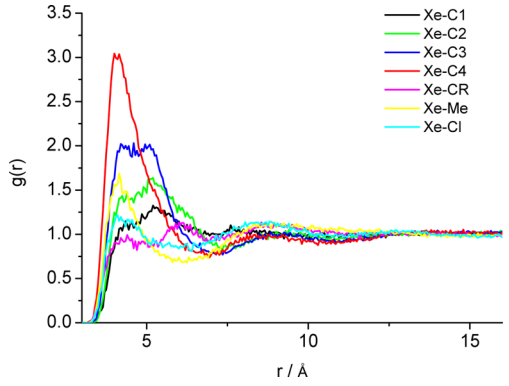

Figure 2. Radial distribution functions, $g(r)$, of Xe with the atoms of [bmim][Cl]. For atom labels, see Figure 1.

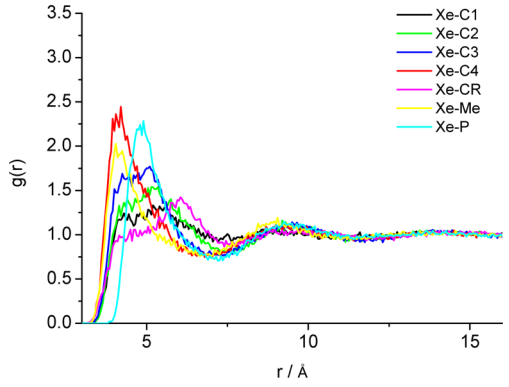

Figure 3. Radial distribution functions, $g(r)$, of Xe with the atoms of [bmim][PF_6]. For atom labels, see Figure 1.

counting each atom at a distance r weighted by its charge. Such a function indicates the average amount of charge at a given distance from Xe. The results are shown in Figure 4.

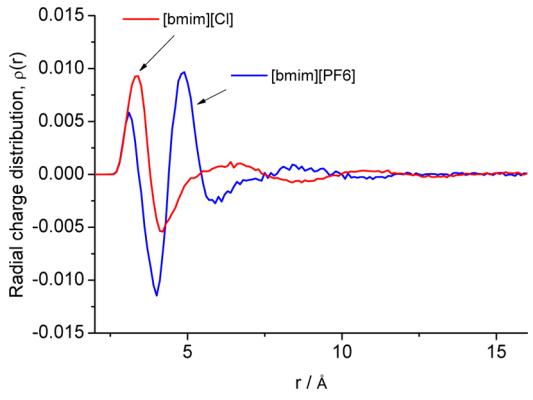

Figure 4. Radial charge distribution function, $\rho(r)$, for Xe with [bmim][X].

In [bmim][PF_6], xenon is surrounded, on average, by a small layer (thickness of about 0.8 Å) of positive charge, likely due to the small amount of charge of the alkyl protons (0.06e each[20,21]), in agreement with the results obtained by the $g(r)$ showing a preferential solvation by the butyl chains. This is followed by a layer of negative charge distribution having a higher intensity, in magnitude, and a larger thickness with likely contributions from the hexafluorophosphate anions. The charge turns again positive at relatively large distances before averaging out, as expected, in the bulk. In [bmim][Cl], the positive layer of charge surrounding the Xe atom is significantly higher in intensity and thicker than the positive layer found in the hexafluorophosphate IL. This difference is in agreement with the lower probability of finding chloride anions in close contact with Xe, with respect to the PF_6^- anions that we can observe in the $g(r)$. Therefore, the average solvation shell of Xe is mainly composed of butyl chains; hexafluorophosphate can also be in close contact because its charge distribution does not prevent it from being in the hydrophobic region. In contrast, the chloride anion approaches the xenon atom with more difficulty because of a less favorable interaction with the alkyl chains, thus leaving, on average, a higher amount of positive charge surrounding Xe. We note that a microsegregation between charged and hydrophobic domains in ILs has been predicted by MD simulations[28,29] and confirmed by experiments,[30,31] already with butyl derivatives, although it clearly becomes more evident with higher homologues.

The structure of Xe@ILs is an interesting example of a system where the cage concept can be applied. The network of ions constituting the cage are, in fact, dominated by strong electrostatic interactions that result in relatively slow dynamics. In contrast, Xe is only affected by van der Waals interactions with its environment; therefore, it is expected to have a significantly faster dynamics within the cage than that of the cage itself. Following Moro et al.,[32] the cage at time t is defined as the ensemble of all ions surrounding the solute Xe atom at a given time t. Thus, at each time step, the cage potential energy, $E_c(\mathbf{r},t)$, is defined as the interaction energy of Xe with the atoms of the cage, assuming that Xe is free to move (its coordinates being given by $\mathbf{r}$) while the remaining ions are frozen at their instantaneous position. This choice allows us to define the cage minimum, $\mathbf{r}_c$, that is, the coordinates where the cage potential energy has a minimum as the position of the Xe atom is varied, keeping the coordinates of the [bmim][X] solvent fixed.

On the basis of this definition of the cage potential, we can calculate the distribution of cage volumes for the two systems. To this end, we created a 3D grid around the minimum of the cage occupied by the Xe atom at each time step, with spacing of 0.1 Å along the x, y, and z directions, and the volume was obtained by adding all cells where the cage potential was lower than $(1/2)k_BT$. This represents the free volume available to the xenon center of mass within its cage, thus excluding the volume of the xenon atom itself. Therefore, the cage volume is not the actual void volume, but it may be considered as a descriptor of the excess volume available to the dissolved gas, and thus, it is strictly related to the average local free volume $\langle v_h \rangle$ mentioned in the Introduction. This aspect should be considered when examining the quantitative data of cage volumes listed in Table 1 and during the discussion of the dependence of the ^{129}Xe chemical shift upon the compression effects (vide ultra). The cage volume distributions for the two systems are shown in

Table 1. Some Parameters of the Two Systems Investigated[a]

Xe@[bmim][X]	$\overline{V}_c$/Å^3	$\overline{q}$ cluster/e	$\overline{\sigma}$/ppm
[Cl]	2.20 ± 0.02	9.4 ± 0.1	5416 ± 17
[PF_6]	2.38 ± 0.02	4.2 ± 0.1	5479 ± 11

[a]Parameters: the average cage volume, $\overline{V}_c$; the average charge of the clusters selected for DFT shielding calculations, $\overline{q}$; the average shielding constant, $\overline{\sigma}$, used to calculate the relative chemical shift variation.

Figure 5, where $f(V_c)$ is the probability to find a cage volume between V_c and $V_c + dV_c$. The results clearly show that small

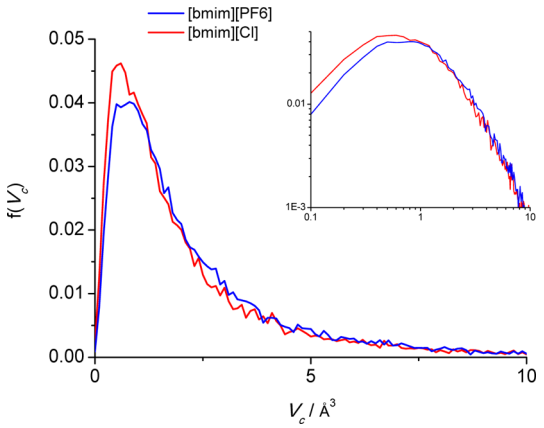

Figure 5. Distribution function, $f(V_c)$, of the volumes of the cage in Xe@[bmim][X]. The same curves are on a log−log plot in the inset.

volumes are more likely for the [Cl] system than for the [PF_6] system, in qualitative agreement with the results of Yu et al.[16] This finding is consistent with the observed ^{129}Xe chemical shift of the two liquids, where the deshielding effects have been ascribed, inter alia, to the compression effects of the cage on the Xe atoms.[8]

The fact that the cage structures of the two systems are clearly, but not largely, different (see Table 1) is in agreement with a xenon cage largely determined by the butyl chains of the common [bmim] cation and perturbed by the anions.

From the trajectory files, we have extracted clusters of molecules centered on the Xe atom. We have included in the clusters all molecules for which at least one atom was within 7.37 Å from the Xe atom. This distance is larger than the first minimum of the $g(r)$ for several Xe−X pairs, which guarantees that the first solvation shell is properly included. Moreover, the average charge modulation is mostly quenched after 7.37 Å; see Figure 4. With very few exceptions, the clusters were positively charged (see Table 1).

3.2. Relativistic DFT Calculations of the ^{129}Xe Chemical Shift. In Figure S1 in the Supporting Information, we show the convergence of the calculated average shielding for the two systems. Although there are large fluctuations in the instantaneous value of the shielding constant, the average value appears to be reasonably converged after including all clusters selected.

The relative chemical shift, $\Delta\delta = \delta_{Xe@[bmim][Cl]} - \delta_{Xe@[bmim][PF6]}$, which has been found experimentally to be ~40 ppm,[8] can be calculated as $\Delta\delta = -\Delta\sigma = \sigma_{Xe@[bmim][PF6]} - \sigma_{Xe@[bmim][Cl]}$ and amounts to 63 ± 20 ppm, where $\sigma_{Xe@[bmim][X]}$ is the average shielding constant of ^{129}Xe in the two ILs obtained from the 21 clusters selected; see Table 1. This result not only has the correct sign but is quite close to the experimental value also in magnitude.

In Figure 6, we show the correlation between the shielding constant and the cage volume. It is noteworthy that only for [bmim][Cl] is there a non-negligible number of cases with a cage volume smaller than about 1 Å^3 (circled in Figure 6) that yield a much lower value of σ. This means that in a significant number of cases, the compression effects exerted by the surrounding cage molecules on the Xe atoms lead to low

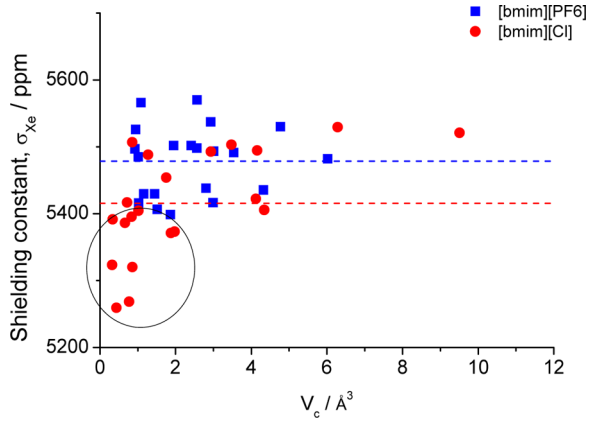

Figure 6. Correlation between the calculated ^{129}Xe shielding constant and the cage volume V_c. Dotted lines are the average shielding constants (see Table 1).

shielding constants (below 5400 ppm), thus significantly contributing to the deshielding of Xe in [bmim][Cl].

We have also verified that the net charge of the cluster does not bias our results; in Figure S2 in Supporting Information, we show the plot of σ(Xe) versus the charge of the clusters, q. It is clear that no correlation exists; in fact, the shielding constant is likely to be affected only by the charge distribution in close contact with xenon (see Figure 1).

4. CONCLUSIONS

We have been able to reproduce the observed shielding effect on ^{129}Xe in [bmim][Cl] and [bmim][PF_6] and to rationalize it as a result of both (i) a different distribution of cage volumes in the two systems, keeping in mind that such volumes represent the free volume available to the Xe atoms within the cage, and not the absolute void volumes, and (ii) a different charge distribution around the cage itself. Narrower cages in [bmim][Cl] produce a larger deshielding because the average charge distribution around Xe is more positive. The harder and more coordinating nature of the Cl^- anion hampers its diffusion within the alkyl chain domains, where xenon is mostly residing, thus allowing for a tighter and closer solvation of Xe by the butyl chains. In contrast, hexafluorophosphate can enter more easily into the hydrophobic domains, thereby disrupting the Xe solvation shell and bringing into the cage an amount of negative charge that has a shielding effect (or less deshielding) in [bmim][PF_6].

The fact that relativistic DFT calculations on clusters extracted from the two trajectories reproduce the observed value of the relative chemical shift (that is, xenon is more shielded, by a few tens of ppm, in [bmim][PF_6] than in [bmim][Cl]) is an indication of the correctness, at least at a qualitative level, of the structure obtained from the classical MD. This is because of the large sensitivity of ^{129}Xe to minor changes in its chemical environment. On the other hand, the expected accuracy of the computational protocol is limited not only by the MD part (classical and nonpolarizable) but also by the many approximations of the DFT part: the level of theory, basis sets, limited size of the clusters and, most important, the limited number of clusters selected due to the fact that such calculations are rather time-consuming. Thus, as we see in Figure S1 of the Supporting Information, the final uncertainty in the average results is quite large. This means that minor variations in the experimental chemical shift of xenon, for

example, comparing $\delta(^{129}Xe)$ in [bmim][Cl] and [bmim][Br], would be beyond the possibility of this approach. However, we believe that the main factors responsible for the xenon shielding, and the way in which they act, have been clearly demonstrated.

Therefore, as previously highlighted on the basis of the experimental data only,[8] the computational results point out that Xe atoms are sensitive probes of even small changes in the local organization of the IL mainly carried out by the anion.

■ ASSOCIATED CONTENT

● Supporting Information

Additional figures, including convergence of the average shielding constant and a plot of the calculated ^{129}Xe shielding constant versus the total charge of the cluster are included. This material is available free of charge viae Internet.

■ AUTHOR INFORMATION

Corresponding Authors

*E-mail: giacomo.saielli@unipd.it (G.S.).
*E-mail: andrea.mele@polimi.it (A.M.).

Notes

The authors declare no competing financial interest.

■ ACKNOWLEDGMENTS

Financial support from MIUR (PRIN 2010N3T9M4, FIRB RBAP11C58Y) and Fondazione CARIPARO (Progetti di Eccellenza "Nano-Mode") is gratefully acknowledged. Calculations were run on the Linux Cluster of the "Laboratorio Interdipartimentale di Chimica Computazionale" of the University of Padova.

■ REFERENCES

(1) Brandt, A.; Grasvik, J.; Hallett, J. P.; Welton, T. Deconstruction of Lignocellulosic Biomass with Ionic Liquids. *Green Chem.* **2013**, *15*, 550−583.

(2) Karadas, F.; Atilhan, M.; Aparicio, S. Review on the Use of Ionic Liquids (ILs) as Alternative Fluids for CO_2 Capture and Natural Gas Sweetening. *Energy Fuels* **2010**, *24*, 5817−5828.

(3) Duan, X.; Ma, J.; Lian, J.; Zheng, W. The Art of using Ionic Liquids in the Synthesis of Inorganic Nanomaterials. *CrystEngComm* **2014**, *16*, 2550−2559.

(4) Armand, M.; Endres, F.; MacFarlane, D. R.; Ohno, H.; Scrosati, B. Ionic-Liquid Materials for the Electrochemical Challenges of the Future. *Nat. Mater.* **2009**, *8*, 621−629.

(5) Matic, A.; Scrosati, B. Ionic Liquids for Energy Applications. *MRS Bull.* **2013**, *38*, 533−537.

(6) Bartik, K.; Luhmer, M.; Dutasta, J.; Collet, A.; Reisse, J. ^{129}Xe and ^{1}H NMR Study of the Reversible Trapping of Xenon by Cryptophane-A in Organic Solution. *J. Am. Chem. Soc.* **1998**, *120*, 784−791.

(7) Morgado, P.; Shimizu, K.; Esperanca José, M. S. S.; Reis, P. M.; Rebelo, L. P. N.; Canongia Lopes, J. N.; Filipe, E. J. M. Using ^{129}Xe NMR to Probe the Structure of Ionic Liquids. *J. Phys. Chem. Lett.* **2013**, *4*, 2758−2762.

(8) Castiglione, F.; Simonutti, R.; Mauri, M.; Mele, A. Cage-Like Local Structure of Ionic Liquids Revealed by a ^{129}Xe Chemical Shift. *J. Phys. Chem. Lett.* **2013**, *4*, 1608−1612.

(9) Canongia Lopes, J. N. A.; Pàdua, A. A. H. Nanostructural Organization in Ionic Liquids. *J. Phys. Chem. B* **2006**, *110*, 3330−3335.

(10) Jameson, C. J.; Sears, D. N.; Murad, S. Molecular Dynamics Averaging of Xe Chemical Shifts in Liquids. *J. Chem. Phys.* **2004**, *121*, 9581−9592.

(11) Yampolskii, Y. P. Methods for Investigation of the Free Volume in Polymers. *Russ. Chem. Rev.* **2007**, *76*, 59−78.

(12) Cadena, C.; Anthony, J. L.; Shah, J. K.; Morrow, T. I.; Brennecke, J. F.; Maginn, E. J. Why is CO_2 so Soluble in Imidazolium-Based Ionic Liquids? *J. Am. Chem. Soc.* **2004**, *126*, 5300−5308.

(13) Huang, X.; Margulis, C. J.; Li, Y.; Berne, B. J. Why is the Partial Molar Volume of CO_2 So Small When Dissolved in a Room Temperature Ionic Liquid? Structure and Dynamics of CO_2 Dissolved in [Bmim][PF_6]. *J. Am. Chem. Soc.* **2005**, *127*, 17842−17851.

(14) Taylor, A. W.; Licence, P.; Abbott, A. P. Non-Classical Diffusion in Ionic Liquids. *Phys. Chem. Chem. Phys.* **2011**, *13*, 10147−10154.

(15) Dlubek, G.; Yu, Y.; Krause-Rehberg, R.; Beichel, W.; Bulut, S.; Pogodina, N.; Krossing, I.; Friedrich, C. Free Volume in Imidazolium Triflimide ([C_3MIM][NTf_2]) Ionic Liquid from Positron Lifetime: Amorphous, Crystalline, and Liquid States. *J. Chem. Phys.* **2010**, *133*, 124502.

(16) Yu, Y.; Beichel, W.; Dlubek, G.; Krause-Rehberg, R.; Paluch, M.; Pionteck, J.; Pfefferkorn, D.; Bulut, S.; Friedrich, C.; Pogodina, N.; Krossing, I. Free Volume and Phase Transitions of 1-Butyl-3-methylimidazolium Based Ionic Liquids from Positron Lifetime Spectroscopy. *Phys. Chem. Chem. Phys.* **2012**, *14*, 6856−6868.

(17) Beichel, W.; Yu, Y.; Dlubek, G.; Krause-Rehberg, R.; Pionteck, J.; Pfefferkorn, D.; Bulut, S.; Bejan, D.; Friedrich, C.; Krossing, I. Free Volume in Ionic Liquids: A Connection of Experimentally Accessible Observables from PALS and PVT Experiments with the Molecular Structure from XRD Data. *Phys. Chem. Chem. Phys.* **2013**, *15*, 8821−8830.

(18) Canongia Lopes, J. N.; Shimizu, K.; Padua, A. A. H.; Umebayashi, Y.; Fukuda, S.; Fujii, K.; Ishiguro, S. A Tale of Two Ions: The Conformational Landscapes of Bis-(trifluoromethanesulfonyl)amide and *N*,*N*-Dialkylpyrrolidinium. *J. Phys. Chem. B* **2008**, *112*, 1465−1472.

(19) Smith, W.; Forester, T. R.; Todorov, I. T. *DL_POLY Classic*, 2010. http://www.ccp5.ac.uk/DL_POLY_CLASSIC (accessed Nov 12, 2014).

(20) Canongia Lopes, J. N.; Deschamps, J.; Padua, A. A. H. Modeling Ionic Liquids Using a Systematic All-Atom Force Field. *J. Phys. Chem. B* **2004**, *108*, 2038−2047.

(21) Canongia Lopes, J. N.; Deschamps, J.; Padua, A. A. H. Modeling Ionic Liquids Using a Systematic All-Atom Force Field. *J. Phys. Chem. B* **2004**, *108*, 11250−11250.

(22) Bohn, M.; Fischer, J.; Kohler, F. Prediction of Excess Properties for Liquid Mixtures: Results from Perturbation Theory for Mixtures with Linear Molecules. *Fluid Phase Equilib.* **1986**, *31*, 233−252.

(23) Bagno, A.; D'Amico, F.; Saielli, G. Computer Simulation of Diffusion Coefficients of the Room-Temperature Ionic Liquid [Bmim][BF_4]: Problems with Classical Simulation Techniques. *J. Mol. Liq.* **2007**, *131*, 17−23.

(24) Yan, T.; Burnham, C. J.; Del Pòpolo, M. G.; Voth, G. A. Molecular Dynamics Simulation of Ionic Liquids: The Effect of Electronic Polarizability. *J. Phys. Chem. B* **2004**, *108*, 11877−11881.

(25) te Velde, G.; Bickelhaupt, F. M.; Baerends, E. J.; Fonseca Guerra, C.; van Gisbergen, S. J. A.; Snijders, J. G.; Ziegler, T. Chemistry with ADF. *J. Comput. Chem.* **2001**, *22*, 931−967.

(26) Ledbetter, M. P.; Saielli, G.; Bagno, A.; Tran, N.; Romalis, M. V. Observation of Scalar Nuclear Spin−Spin Coupling in Van Der Waals Complexes. *Proc. Natl. Acad. Sci. U.S.A.* **2012**, *109*, 12393−12397.

(27) Bagno, A.; Saielli, G. Understanding the Extraordinary Deshielding of ^{129}Xe in a Permetallated Cryptophane by Relativistic DFT. *Chem.—Eur. J.* **2012**, *18*, 7341−7345.

(28) Wang, Y.; Voth, G. A. Unique Spatial Heterogeneity in Ionic Liquids. *J. Am. Chem. Soc.* **2005**, *127*, 12192−12193.

(29) Urahata, S. M.; Ribeiro, M. C. C. Structure of Ionic Liquids of 1-Alkyl-3-methylimidazolium Cations: A Systematic Computer Simulation Study. *J. Chem. Phys.* **2004**, *120*, 1855−1863.

(30) Xiao, D.; Rajian, J. R.; Cady, A.; Li, S.; Bartsch, R. A.; Quitevis, E. L. Nanostructural Organization and Anion Effects on the Temperature Dependence of the Optical Kerr Effect Spectra of Ionic Liquids. *J. Phys. Chem. B* **2007**, *111*, 4669−4677.

(31) Triolo, A.; Russina, O.; Bleif, H.; Di Cola, E. Nanoscale Segregation in Room Temperature Ionic Liquids. *J. Phys. Chem. B* **2007**, *111*, 4641−4644.
(32) Moro, G. J.; Nordio, P. L.; Noro, M.; Polimeno, A. A Cage Model of Liquids Supported by Molecular Dynamics Simulations. I. the Cage Variables. *J. Chem. Phys.* **1994**, *101*, 693−702.